# Contributions of Residues of Pancreatic Phospholipase $A_2$ to Interfacial Binding, Catalysis, and Activation†

Bao-Zhu Yu,‡ Joseph Rogers,‡ Ming-Daw Tsai,§ Charles Pidgeon,|| and Mahendra Kumar Jain*,‡

*Department of Chemistry and Biochemistry, University of Delaware, Newark, Delaware 19716, Departments of Chemistry and Biochemistry and Ohio State Biochemistry Program, The Ohio State University, Columbus, Ohio 43210, and Department of Medicinal Chemistry, School of Pharmacy, Purdue University, West Lafayette, Indiana 47907*

*Received September 14, 1998; Revised Manuscript Received December 10, 1998*

ABSTRACT: Primary rate and equilibrium parameters for 60 site-directed mutants of bovine pancreatic phospholipase $A_2$ (PLA2) are analyzed so incremental contributions of the substitution of specific residues can be evaluated. The magnitude of the change is evaluated so a functional role in the context of the N- and C-domains of PLA2 can be assigned, and their relationship to the catalytic residues and to the i-face that makes contact with the interface. The effect of substitutions and interfacial charge is characterized by the equilibrium dissociation constant for dissociation of the bound enzyme from the interface ($K_d$), the dissociation constant for dissociation of a substrate mimic from the active site of the bound enzyme ($K_L$*), and the interfacial Michaelis constants, $K_M$* and $k^*_{cat}$. Activity is lost (>99.9%) on the substitution of H48 and D49, the catalytic residues. A more than 95% decrease in $k^*_{cat}$ is seen with the substitution of F5, I9, D99, A102, or F106, which form the substrate binding pocket. Certain residues, which are not part of the catalytic site or the substrate binding pocket, also modulate $k^*_{cat}$. Interfacial anionic charge lowers $K_d$, and induces $k^*_{cat}$ activation through K56, K53, K119, or K120. Significant changes in $K_L$* are seen by the substitution of N6, I9, F22, Y52, K53, N71, Y73, A102, or A103. Changes in $K_M$* [$=(k_2+k_{-1})/k_1$] are attributed to $k^*_{cat}$ ($=k_2$) and $K_L$* ($=k_{-1}/k_1$). Some substitutions change more than one parameter, implying an allosteric effect of the binding to the interface on $K_S$*, and the effect of the interfacial anionic charge on $k^*_{cat}$. Interpreted in the context of the overall structure, results provide insights into the role of segments and domains in the microscopic events of catalytic turnover and processivity, and their allosteric regulation. We suggest that the interfacial recognition region (i-face) of PLA2, due to the plasticity of certain segments and domains, exercises an allosteric control on the substrate binding and chemical step.

The kinetic scheme (Scheme 1) for interfacial catalysis has provided a general basis for analyzing the function of phospholipase $A_2$ (PLA2)[1] in terms of the primary rate and equilibrium parameters with microscopic functional and mechanistic significance (*1*−*10*). A resolution of the catalytic and two-dimensional processivity parameters requires constraining the experimental conditions, such that the contribution of the variables can be quantitatively evaluated to ensure that the microscopic steady-state condition is satisfied during the reaction progress. To keep the chemical step rate-limiting (*8*), the exchange rates for the reactants and products between the coexisting interfaces should be such that the substrate replenishment does not become rate-limiting (*9*). Within such constraints, intrinsic properties of lipid−water interfaces permit kinetic analysis in two extreme limits where the

Scheme 1: Kinetic Model for Interfacial Catalysis That Shows Relationships between the Primary Rate and Equilibrium Parameters[a]

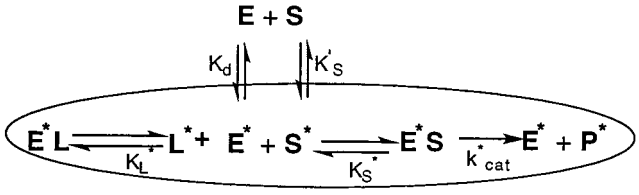


[a] In this adaptation of the Michaelis scheme, the species in the interface are marked with an asterisk. Binding of calcium and an equilibrium between the species in the aqueous phase and the interface are inherent in this scheme. The parameters (units) are defined as follows. $K_L$* is the dissociation constant for dissociation of L (=MJ33 or DTPM) from E*L (mole fraction). $K_d$ is the dissociation constant at which half the enzyme is in the interface in the E* form (millimolar). $K_S'$ is the critical micelle concentration, or the partition constant at which half the substrate is bound to the interface. $K_S$* is the dissociation constant for E*S (mole fraction), which also equals $k_{-1}/k_1$, the ratio of the dissociation and association rate constants. $k^*_{cat}$ is the rate constant for the rate-limiting chemical step, $k_2$ ($s^{-1}$). $K_M$* is the interfacial Michaelis constant [$=(k_{-1}+k_2)/k_1$] (mole fraction).

† This work was supported by PHS (Grant GM29703 to M.K.J. and Grant GM41788 to M.-D.T.).

* Corresponding author. E-mail: mkjain@udel.edu.

‡ University of Delaware.

§ The Ohio State University.

|| Purdue University.

[1] Abbreviations: cmc, critical micelle concentration; $DC_7PC$, 1,2-diheptanoyl-*sn*-3-glycerophosphocholine; deoxy-LPC, 1-hexadecylpropanediol-3-phosphocholine; DMPM, 1,2-dimyristoyl-*sn*-3-glycerophosphomethanol; DTPM, 1,2-ditetradecyl-*sn*-3-glycerophosphomethanol; i-face, interfacial recognition region of PLA2 that comes in contact with the substrate interface; L, active site-directed substrate mimic such as a substrate, product, or competitive inhibitor; MJ33, 1-hexadecyl-3-(trifluoroethyl)-*rac*-glycero-2-phosphomethanol; PLA2, phospholipase $A_2$ from bovine pancreas unless noted otherwise. Relationships between the rate and equilibrium constants are defined in Scheme 1 and developed elsewhere (*3*, *5*−*7*).

10.1021/bi982215f CCC: $18.00 
Published on Web 03/25/1999

chemical step remains rate-limiting. In the scooting mode, the binding of PLA2 to DMPM vesicles is an irreversible pre-steady-state event, and the catalytic turnover by E* occurs with virtually infinite processivity until all the substrate present in the enzyme-containing vesicle is exhausted (*1*, *5*). Excess vesicles are not hydrolyzed because the reactants (E*, S, and P) do not exchange between the vesicles. In the other limit, the substrate and product exchange rapidly compared to the catalytic turnover on the enzyme-containing micelle, as with micelles of a short chain phospholipid, $DC_7PC$ (*6*). The fast exchange condition also applies to rapidly exchanging soluble substrates that partition in an enzyme-containing interface of a diluent (*7*).

We have established methods for characterizing primary interfacial catalytic and processivity parameters under the scooting (*3*, *5*) and fast exchange (*6*, *7*) limits of Scheme 1. The binding of the enzyme to the interface, characterized by $K_d$, is unequivocally dissected from the catalytic turnover parameters. The calcium-dependent dissociation constants for active site-directed substrate mimics, $K_L$* ($K_I$*, $K_P$*, and $K_S$* for I, P, and S, respectively), are related to the affinity for the active site of E*. The interfacial Michaelis parameters, $K_M$* and $k^*_{cat}$, characterize the processive catalytic turnover at the interface. In this analysis, interfacial activation is a positive allosteric effect of the interface on the binding of ligand to the active site of E*, $K_L$* (*2*), and also the effect of the anionic surface charge on the chemical step, $k^*_{cat}$ (*6*).

Having established protocols for the resolution of the interfacial kinetic parameters with well-defined microscopic significance, we now focus our attention on relationships of such parameters to structural features of PLA2. Catalysis is a molecular property of the whole enzyme in which the proximal residues, as well as distal segments and domains, contribute to the events of catalytic turnover and processivity. The identity of residues in contact with substrate mimics in cocrystals (*10*−*13*), coupled with biochemical (*14*−*19*) and spectroscopic (*20*−*22*) information, provides a reasonable starting point for the interpretation of the kinetic results (*3*, *13*, *23*, *24*). This strategy has established a role for the H48/D99 dyad in the chemical step (*12*, *14*), for D49 in calcium binding (*25*), and for F5, F22, and F106 in substrate binding (*26*, *27*) and an obligatory requirement for calcium in the substrate binding (*17*) and chemical step (*19*). Collectively, these results provide a consensus basis for the catalytic mechanism (*19*). Also, the i-face residues and domains, which come in contact with the substrate interface (*28*−*30*) and exert an allosteric control on the steps of the catalytic cycle (*31*), are tentatively identified.

In this paper, we report a set of parameters (Table 1) for 60 site-directed mutants of bovine pancreatic PLA2. The effect of substitutions on $K_d$, $K_L$* (DTPM and MJ33), and $K_M$* and $k^*_{cat}$ for $DC_7PC$ and DMPM is analyzed. The magnitude of the change in a specific parameter relative to that of WT (entry 1 in Table 1) is interpreted in the context of the overall structure to gain insight in the binding, catalysis, and allosteric steps. Often, individual substitutions influence only certain parameters (*24*−*26*, *32*−*35*), and the topography of the distribution of such residues permits identification of segments and domains that control specific microscopic events. As a first approximation, four structural features of PLA2 (Figure 1) are useful.

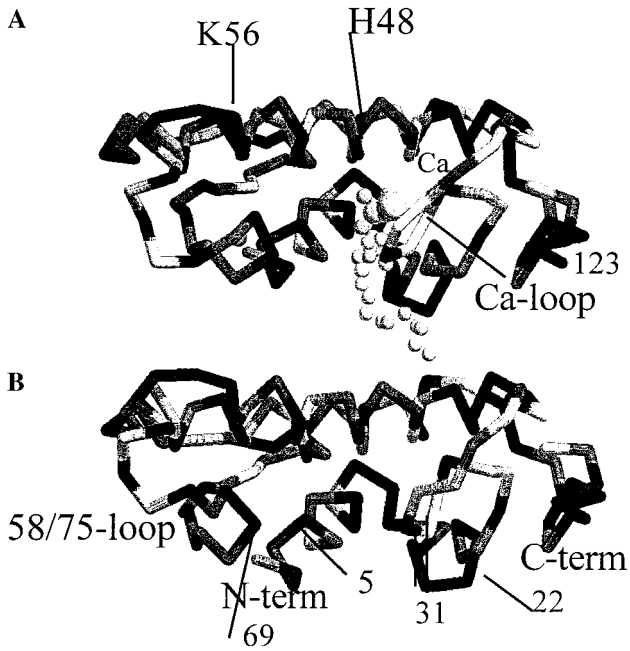


FIGURE 1: Backbone structure of (A) the complex with MJ33 (E·Ca·MJ33) obtained from the crystal structure (PDB file 1FDK from ref *3*) and (B) the NMR structure of the E·Ca form (*20*). Features of interest include the substrate binding site in the slot between two domains; the C-terminus of the 123-residue chain of PLA2 and the calcium binding loop (residues 28−32) are on the right domain, and the N-terminus is in the left domain. The alkyl chain of MJ33 bound through calcium protrudes from the active site. The consensus interfacial recognition surface of PLA2, the i-face, is on the lower end of the PLA2 molecule along the plane perpendicular to the plane of the paper; the methyl end of the inhibitor chain would dip in the interface. Several residues of interest are also marked. The H-bonding network in the left N-domain connecting A1, Q4, P68, Q71, Y52, Y73, and D99 and a highly conserved water molecule forming a bond to the catalytic dyad D99/H48 are not shown.

(a) The C-domain to the right consists of the C-terminal segment connected to the calcium loop of residues 25−36 through a disulfide bridge of residues 27−123 (*36*).

(b) In the N-domain, the loop of residues 58−75 connects two relatively stable helices (residues 41−57 and 76−91) on the top surface. Also, the N-terminal segment is connected through the H-bonding network with a highly conserved water through A1, Q4, P68, Q71, Y52, Y73, and D99 (*23*).

(c) At the junction of the N- and C-domains lie the H48/D99 dyad and D49, which together with calcium make up the catalytic site (*14*, *19*). Residues 26−35 form the EF loop to provide three ligands for the calcium binding.

(d) The i-face residues are on the lower face of the C- and N-domains (*34*, *40*), where the hydrophobic residues (L2, W3, F5, I9, F22, L31, 63−65, and Y69) at the entrance to the active site slot form a close contact with the upper end of the acyl chains of the substrate. Thus, the i-face makes multiple contacts along the horizontal plane with about 30 phospholipid molecules (*1*, *37*, *38*, *40*). It is involved in $K_S$* allosteric activation (*2*, *6*). Also, the cationic residues (K53, K56, K120, and K121), farther away from the slot, are responsible for $k^*_{cat}$ activation (*31*).

## EXPERIMENTAL PROCEDURES

$DC_7PC$ was from Avanti Polar Lipids. MJ33 (*41*), DTPM (*42*), and DMPM (*1*) were synthesized. All other reagents

Table 1: Equilibrium Binding and Kinetic Parameters[a] for Bovine Pancreatic PLA2 Mutants

| | | | | | | | | DC$_7$PC | | | | | |
|---|---|---|---|---|---|---|---|---|---|---|---|---|---|
| | | IAM $t_R$ (min) | | | | DMPM | | 0.001 M NaCl | | | 4 M NaCl | | |
| | PLA2 | isocratic | gradient | $K_S$*(DTPM) | $K_I$*(MJ33) | $\nu_o$ | $K_M$* | $V_M^{app}$ | $K_M^{app}$ | $K_M$* | $V_M^{app}$ | $K_M^{app}$ | $K_M$* |
| 1 | WT | 0.53 | 9.9 | 0.02 | 0.009 | 330 | 0.65 | 30 | 2.3 | >1 | 850 | 0.2 | 0.99 |
| 2 | L2A | 0.18 | 5.6 | 0.023 | 0.01 | 100 | 0.1 | 7 | 0.8 | 0.11 | 350 | 0.24 | 0.26 |
| 3 | L2R | 0.07 | 7.8 | | | <1 | | | | | 1.5 | | |
| 4 | L2W | 1.3 | 10 | 0.043 | 0.016 | 10 | 0.1 | 13 | 5.0 | 0.1 | 155 | 0.14 | 0.1 |
| 5 | W3A | 0.05 | 7.8 | 0.06 | 0.04 | 80 | 3.3 | 10 | 6.5 | >1 | 210 | 1.15 | 2.7 |
| 6 | Q4A | 0.15 | 5.1 | 0.06 | 0.011 | 185 | 1.5 | 11 | 4.3 | 1.3 | 340 | 0.22 | 0.8 |
| 7 | Q4E | 0.2 | 7.8 | | | 220 | | | | | | | |
| 8 | Q4K | 0.32 | 7.6 | 0.025 | 0.006 | 130 | 0.3 | 1 | | | 130 | 0.41 | 0.23 |
| 9 | Q4N | 0.63 | 10.8 | | | 105 | | | | | | | |
| 10 | F5A | 0.21 | 7.8 | | | 2 | | <1 | | | 4 | | |
| 11 | F5V | 0.2 | 7 | 0.005 | 0.003 | 2 | 0.33 | | | | | | |
| 12 | F5W | 1.9 | 11.5 | | | 3 | | | | | | | |
| 13 | F5Y | 0.81 | 9.3 | | | 4 | | | | | | | |
| 14 | N6A | 3.8 | 10 | >0.2 | 0.006 | 320 | 0.85 | 40 | 2.3 | 1.4 | 735 | 0.06 | 0.4 |
| 15 | N6D | 2.2 | 10.1 | | | 380 | | | | | | | |
| 16 | I9A | 0.47 | 8.2 | 0.032 | 0.0037 | 50 | 0.16 | 1 | | | 52 | 0.19 | 0.15 |
| 17 | I9F | 0.13 | 7.5 | >0.1 | 0.02 | 20 | 1.7 | <1 | | | 10 | 0.14 | 0.31 |
| 18 | I9S | 0.17 | 7.5 | | | 22 | | | | | | | |
| 19 | I9Y | 0.16 | 4.9 | | | 6 | | <1 | | | 6 | 0.046 | |
| 20 | F22A | 0.02 | 7.1 | 0.11 | 0.03[a] | 30 | 0.25 | <1 | | | 11 | 0.31 | 0.28 |
| 21 | F22I | 0.76 | 9.3 | 0.054 | 0.006 | 190 | 0.18 | 5 | 1.7 | 0.24 | 145 | 0.16 | 0.6 |
| 22 | F22Y | 0.9 | 10 | 0.35 | 0.016 | 200 | 1.3 | 23 | 3.1 | >1 | 320 | 0.08 | 1.8 |
| 23 | C27A/C123A | 0.43 | 8.6 | >0.1 | 0.082 | 90 | ≫1 | <1 | | | 220 | 0.1 | ≫1 |
| 24 | H48A | 0.2 | 6.6 | | | <1 | | | | | | | |
| 25 | H48N | 0.24 | 6.5 | | | <1 | | | | | | | |
| 26 | H48Q | 0.14 | 7.1 | | | <1 | | | | | | | |
| 27 | D49A | 2.9 | 12.3 | | | <1 | | | | | | | |
| 28 | D49E | 0.73 | 10.4 | | | <1 | | | | | | | |
| 29 | D49K | 3.5 | 13.8 | | | <1 | | | | | | | |
| 30 | D49N | 2.7 | 12.6 | | | <1 | | | | | | | |
| 31 | D49Q | 4.1 | 13.6 | | | <1 | | | | | | | |
| 32 | C51A/C98A | 0.61 | 9.3 | 0.001 | 0.042 | 460 | 0.14 | 18 | 1.9 | 0.4 | 340 | 0.15 | 0.32 |
| 33 | Y52F | 0.01 | 8.7 | 0.08 | 0.006 | 330 | 1.4 | 15 | 1.5 | 0.27 | 400 | 0.12 | 0.37 |
| 34 | Y52K | 0.1 | 7.6 | | | 6 | | <1 | | | 2 | | |
| 35 | Y52V | 0.16 | 7.3 | 0.2 | 0.22 | 90 | >1 | <1 | | | 30 | 0.2 | >1 |
| 36 | K53I | 0.47 | 10.6 | 0.007 | 0.004 | 340 | 0.18 | 110 | | | 880 | | 0.3 |
| 37 | K53M | 0.2 | 10.8 | 0.12 | 0.008 | 240 | >1 | 230 | 1.3 | 0.95 | 1100 | 0.2 | 0.7 |
| 38 | K56E | 0.26 | 10.4 | >0.1 | 0.007 | 230 | 0.75 | 45 | 1.3 | 0.96 | 1200 | 0.25 | 1 |
| 39 | K56F | 3.0 | 15.3 | 0.003 | 0.003 | 330 | 0.16 | 130 | | | 1100 | | 0.23 |
| 40 | K56I | 2.7 | 13.9 | 0.006 | 0.005 | 250 | 0.38 | 140 | | | 1300 | | 0.18 |
| 41 | K56M | 2.2 | 13.8 | 0.01 | 0.004 | 280 | 0.42 | 400 | 0.75 | 0.44 | 1400 | 0.26 | 0.7 |
| 42 | K56N | 0.04 | 10.9 | 0.004 | 0.003 | 340 | 0.14 | 140 | | | 750 | | 0.11 |
| 43 | K56T | 0.06 | 10.8 | 0.007 | 0.008 | 270 | 0.76 | 130 | | | 500 | | 0.27 |
| 44 | N71E | 0.3 | 6.4 | >0.1 | 0.002 | 150 | 0.16 | 2 | | | 72 | 0.22 | 0.047 |
| 45 | Y73A | 0.06 | 10.1 | | | 195 | | 0.7 | | | 25 | 0.46 | |
| 46 | Y73F | 0.6 | 8.6 | 0.22 | 0.014 | 290 | 1.3 | 25 | 4.7 | | 310 | 0.43 | 0.81 |
| 47 | Y73K | 0.11 | 10.3 | | | 30 | | | | | 2 | | |
| 48 | Y73S | 0.11 | 12.5 | | | 75 | | <1 | | | 35 | 0.83 | |
| 49 | Y52F/Y73F | 0.27 | 6.7 | 0.1 | 0.02 | 260 | 0.59 | 7 | 1.8 | 1.2 | 280 | 0.078 | 1.7 |
| 50 | D99A | 0.17 | 7.4 | | | <1 | | | | | | | |
| 51 | D99N | 0.2 | 7.9 | 0.003 | 0.005 | 20 | 0.14 | 0.25 | 5.5 | 0.14 | 10 | 0.44 | 0.21 |
| 52 | D99N/Y52F/Y73F | 0.05 | 5.9 | >0.1 | 0.01 | 11 | 2.3 | 0.1 | 4.1 | 0.17 | 5.4 | 0.15 | 0.3 |
| 53 | A102I | 0.37 | 6.9 | >0.1 | 0.034 | 60 | 0.42 | 1.5 | | | 30 | 0.185 | 0.8 |
| 54 | A102S | 1.2 | 8.9 | 0.02 | 0.018 | 95 | 0.08 | 12 | 1.5 | >1 | 90 | 0.06 | 0.32 |
| 55 | A103S | 1.6 | 10.3 | 0.2 | 0.022 | 170 | 1.3 | 21 | 0.28 | >1 | 230 | 0.085 | 5.2 |
| 56 | F106A | 0.11 | 6.9 | | 0.18 | 100 | 0.45 | 9 | 3.2 | | 80 | 0.07 | 0.66 |
| 57 | F106I | 0.71 | 9.3 | 0.07 | 0.02 | 155 | 0.67 | 4.5 | | | 92 | 0.12 | 0.35 |
| 58 | F106Y | 0.53 | 9.2 | | 0.02 | 45 | 0.26 | <1 | | | 10 | 0.07 | 2.1 |
| 59 | K120A/K121A | 0.64 | 9.5 | 0.01 | 0.004 | 90 | 0.66 | 50 | 1.9 | 0.98 | 600 | 0.12 | 0.61 |
| 60 | Δ115−123/C27A | 0.44 | 9.2 | 0.21 | 0.35 | 30 | >1 | <1 | | | 83 | 0.13 | >1 |

[a] The retention times on the IAM column in 1 mM NaCl (column 3) or in a reverse gradient of NaCl (column 4) are related to the binding equilibrium of PLA2 at the interface, E to E*. The dissociation constants, $K_S$*(DTPM) (column 5) and $K_I$*(MJ33) (column 6), are a measure of the affinity of the two mimics for the active site of the E* form. $K_M$*s for DMPM (column 8) or DC$_7$PC (columns 12 and 15) are kinetic parameters for the two substrates. The rates at the maximum mole fraction of the substrate ($X_S = 1$) ($\nu_o$ and $V_M^{app}$ in columns 7 and 12, respectively) are used to calculate $k^*_{cat}$ for the catalytic turnover rate at the interface (eq 1). $K_S$*, $K_I$*, and $K_M$* are in mole fraction; $\nu_o$ and $V_M^{app}$ are in $s^{-1}$.

were analytical grade. Bovine PLA2 mutants were kindly provided by J. Noel, C. Dupureur, Y. Li, B. Huang, X. Liu, and H. Zhu (all from The Ohio State University). Their construction and structural and preliminary kinetic characterization in the scooting mode on DMPM vesicles have been described before: K53 and K56 (*31*, *32*), Y52 and Y73 (*26*,

*43*), F22 and F106 (*27*), H48 (*33*), D49 (*25*), cysteine substitutions (*34*), the H48/D99 pair (*12*, *33*, *44*), and N-terminal (*35*) and C-terminal segments (*36*). Crystallographic results also show that the backbone structure of these mutants is comparable to that of WT, and local structural perturbations are largely in orientations of the N-terminus and of the side chains.

*Kinetic Protocols.* The analytical formalism and experimental protocols used for this study were established previously (*3*, *5*, *6*). Only salient details are given below. Hydrolysis in the scooting mode on DMPM vesicles (*1*, *3*), or the hydrolysis of $DC_7PC$ micelles under the rapid exchange conditions (*6*), was monitored by the pH-stat method. Typically, real-time titration of released fatty acid was carried out in 1 mM $CaCl_2$ and 1 mM NaCl at 25 °C and pH 8.0 under a stream of nitrogen with a Brinkman (Metrohm) or Radiometer titrator with 3 mM NaOH as the titrant. The reaction was initiated by the addition of 0.1−30 pmol of PLA2 in a volume of 1−30 $\mu$L. Soluble inhibitor MJ33, if present, was added after initiating the reaction; however, the order of addition makes little difference. The titration efficiency under specified conditions was determined by adding a known amount of myristic acid or heptanoic acid to the reaction mixture in the absence of PLA2. The rate parameters are expressed as turnover number in $s^{-1}$. Uncertainty in the measured parameters is 10%, and parameters derived from curve fitting have a standard deviation of up to 30%.

In accord with eqs 1−3, hydrolysis of DMPM in the scooting mode is parametrized as $K_M$* and $\nu_o$ (*5*), and the hydrolysis of $DC_7PC$ micelles under the fast exchange conditions as $K_M^{app}$ and $V_M^{app}$ (*6*). By definition, $V_M^{app}$ is equal to $\nu_o$ at $X_S = 1$ (eq 1). $K_M^{app}$ is related to $K_d$ and $K_M$* (eq 3). In Table 1, the apparent kinetic parameters for the hydrolysis of $DC_7PC$ micelles at 1 mM NaCl are given in columns 9−11, and at 4 M NaCl in columns 12−14. As described below, $K_M$* is measured from the inhibition results (eq 2), and $K_d$ and $K_I$* are determined independently as described below.

$$\nu_0 = V_M^{app} = \frac{k_{cat}}{1 + K_M^*} \quad (1)$$

$$\frac{\nu_0}{\nu_I} = 1 + \left(\frac{1 + \frac{1}{K_I}}{1 + \frac{1}{K_M}}\right)\left(\frac{X_I}{1 - X_I}\right) \quad (2)$$

$$V_M^{app} = \frac{K_d K_M}{1 + K_M}\left(1 + \frac{K'_S}{K_M}\right) \quad (3)$$

*Determination of $K_L$*.* The time course of inactivation of PLA2 by alkylation of catalytic His48 provides a quantitative measure of the occupancy of the active site. It permits determination of the dissociation constant, $K_L$*, for the ligand at the active site (*17*, *45*). The 0.03 mL alkylation reaction mixture in a 6 mm × 50 mm borosilicate glass tube consisted of 0.1−1 $\mu$M PLA2 in 50 mM cacodylate buffer at pH 7.3 with 0.1 M NaCl, 0.5 mM $CaCl_2$, 0.03 mg of $\gamma$-globulin, and 2 mM *p*-nitrophenacyl bromide (2-bromo-4′-nitroacetophenone) at 23 °C. For $K_L$* determinations, the incubation mixture also contained the mimic and 1.65 mM deoxy-LPC as the neutral diluent. Recall that a neutral diluent provides a micellar interface for the binding of PLA2, but deoxy-LPC does not bind to the active site of the bound enzyme. At various time intervals, an aliquot of the incubation mixture containing 0.01−10 pmol of enzyme was added to 1.5 mL of the fluorescent lipid assay solution containing 1 $\mu$g of 1-palmitoyl-2-pyrenedecanoylglycero-3-phosphomethanol (Molecular Probes), 250 $\mu$g of bovine serum albumin (Sigma), 0.1 M NaCl, 0.25 mM $CaCl_2$, and 50 mM Tris buffer at pH 8.5 and 23 °C (*17*, *18*, *46*). The assay mixture was pre-equilibrated for 2−3 min to stabilize the baseline before the addition of the aliquot from the alkylation solutions. Residual activity was obtained from the slope of the increase in the fluorescence at 396 nm (excitation at 345 nm on an SLM 4800S spectrofluorimeter) at each time interval.

*Chromatographic Protocols for Interfacial Binding of PLA2*. The HPLC protocol for which the IAM.PC.DD column was used provided a rapid and sensitive method for obtaining a measure of $K_d$, which is proportional to the reciprocal of the retention time ($t_R$), defined as the elution time minus the void time ($t_o = 0.97$ min with a flow rate of 0.5 mL/min), including the dead time through the plumbing (0.3 min). Two sets of conditions were used for elution. The isocratic elution buffer consisted of 1 mM NaCl in 10 mM Tris at pH 8.0. For the reverse gradient, the column was equilibrated in 2 M NaCl in 10 mM Tris at pH 8.0, and the NaCl concentration was lowered linearly to 1 mM between 2 and 7 min.

The IAM-PC stationary phase consists of silica beads covalently close-packed with a monolayer of decylphosphocholine; i.e., each amphiphile molecule is attached via the methyl terminus of the alkyl chain, and the degree of close packing is enhanced by hydrophobic end capping (*47*, *48*). The immobilized monolayer on the surface of the silica beads resembles the interface of phosphatidylcholine vesicles or micelles, except that individual amphiphiles in the matrix cannot be dislodged; thus, the active site of bound PLA2 is not occupied. Elution profiles were monitored at a flow rate of 0.5 mL/min in 10 mM Tris at pH 7.4 with Rainin HPLC hardware sequentially equipped with an absorbance and a fluorescence detector. We have obtained comparable results with several batches of the columns made at Purdue University and the commercially available (model 777007, Regis Technologies, Morton Grove, IL) IAM columns. However, there was considerable variability in the commercially available columns. In our experience, the stability of IAM-PC columns is erratic, and their deterioration is more rapid in a salt gradient. The loss of column integrity is accompanied by a change in the peak shape and its position. Buildup of negative charge on the column is also indicated by an increased level of retention of cationic peptides and tris(2,2′-bipyridine)ruthenium chloride (*49*). For the results listed in Table 1, acceptable uncertainty in the $t_R$ value for WT PLA2 with the gradient elution was taken to be within 0.5 min through the useful life of the column.

## RESULTS

The effect of amino acid substitutions in bovine PLA2 on the microscopic steps in Scheme 1 is evaluated in terms of the parameters summarized in Table 1. The significance of these parameters is evaluated in relation to the NMR and

X-ray structures (Figure 1). Binding of substrate mimics to the active site does not significantly alter the crystallographic backbone structure (*10*, *11*, *13*). In cases where such information is available (*12*, *25*−*27*, *33*−*36*, *43*, *44*), crystallographic and NMR results show only local perturbations at the site of substitution in the mutants. As discussed later, a comparison with the solution structure (*20*) suggests that the crystallographic structure of the enzyme with a mimic in the active site may be closer to the yet unknown structure of PLA2 at the interface.

For the interpretation of the kinetic parameters, we emphasize not only the position of a residue but also its functional relationship to segments and domains that connect the active site to the i-face. One of the serious concerns in the site-directed mutagenesis studies is whether it is justified to directly correlate the functional changes with the structural changes. While such a correlation is a common practice, it is often unwarranted since a large change in the structure may not necessarily lead to a proportional change in function or mechanism, whereas a minor change in structure could have a relatively profound effect. This problem can be avoided by analysis of incremental changes exhibited by a number of mutants. To evaluate the effect of amino acid substitution, parameters obtained under two different sets of conditions are compared on the log−log scale. Such a relationship to the underlying free energy term is useful for assessing the linear incremental contribution of the substitutions relative to WT (entry 1 in Table 1). With a 30% standard deviation in the derived parameters, only more than 3-fold (±0.4 log unit) changes are considered significant for the purposes of comparison.

*Contributions to the Binding of PLA2 to the Interface*. The E to E* step is a recognition event along the i-face of the enzyme that makes contact with the substrate interface (*39*, *40*). In the past, we used a set of protocols, based on the change in the Trp3 fluorescence (*1*, *28*, *45*, *50*), to quantify the bound enzyme and to distinguish the E* form from the E*L form. These methods are not well suited to a case where the intrinsic fluorescence of the protein changes due to a change in the neighboring internal quenchers. We have developed a rapid HPLC method on the IAM-PC column for monitoring the E to E* equilibrium without complications from the occupancy of the active site (*6*). The stationary phase of the IAM-PC column consists of a close-packed monolayer of alkylphosphocholine molecules covalently attached to the derivatized silica bead surface (*47*); thus, the surface resembles the surface of vesicles or micelles for the binding of PLA2. Its advantage lies in the fact that the covalently immobilized amphiphile cannot be dislodged by the bound enzyme; i.e., the E*L type of species is not formed, unless of course a mimic (L) is noncovalently partitioned into the interface. The binding is assessed as the retention time ($t_R$ = elution time − $t_o$) relative to the void volume.

Changes in $t_R$ under a variety of conditions suggest specificity of the interactions of the i-face of PLA2 with the stationary phase. For example, the retention time does not change in the presence of calcium. Since calcium is an obligatory cofactor for the binding of substrate mimics to the active site of PLA2 (*17*), we rule out involvement of the occupancy of the active site. In contrast, as expected, if an inhibitor like MJ33 is partitioned into the column, $t_R$ increases significantly only in the presence of calcium. Also, the

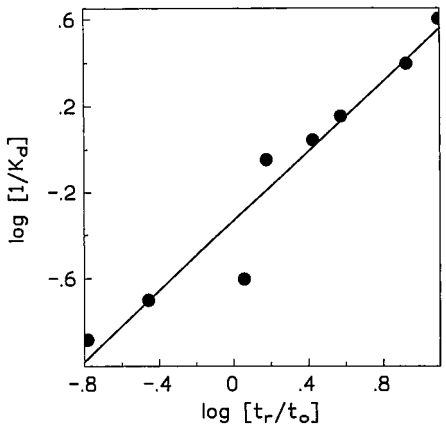


FIGURE 2: Relationship between retention time ($t_R/t_o$) on the IAM column under isocratic conditions at varying NaCl concentrations and reciprocal of the $K_d$ values (millimolar) for the bovine WT.

retention times on the IAM column do not correlate with those on a reverse phase column. For example, the elution time from a 25 mM Vydec $C_4$ column with an acetonitrile gradient (20 to 80% v/v between 5 and 25 min after injection) was 12.7 min for WT and 13.0 min for K56M, compared to a 4-fold change on the IAM column under isocratic conditions (Table 1).

As shown by direct binding and kinetic studies (*6*), an intriguing feature of the binding of PLA2 to zwitterionic interface is that the binding is enhanced at higher NaCl concentrations. The salting-in of PLA2 is largely due to the hydrophobic component of the binding, and a part may be attributed to ionic effects on the enzyme and the interface. As shown in Figure 2, lower $K_d$ values on deoxy-LPC and longer $t_R$ values on the IAM-PC column under isocratic conditions follow the expected proportionality of $1/K_d$ to $t_R$ at several concentrations of NaCl. A slope of 0.82 suggests that comparable factors contribute to the binding of PLA2 at the two zwitterionic surfaces.

The isocratic elution times for the mutants in 1 mM NaCl are in the 0−5 min range (column 3), compared to 5−15 min (column 4 in Table 1) for the elution in the reverse gradient. The isocratic and gradient $t_R$ values are compared in Figure 3. A linear relationship for most mutants implies a direct relationship between the gradient and isocratic $t_R$; i.e., most substitutions induce a comparable change in the interactions under the two sets of conditions. On the basis of the position of the arbitrary diagonal in Figure 3, the gradient $t_R$ is higher by about 9 min. As a possible reason for this delay, it is likely that a complete removal of NaCl from the column takes 2−4 void volumes beyond the end of the gradient at 7 min.

Only the mutants, well-separated from WT (entry 1 in Table 1) in Figure 3, imply a significant role for such residues in the binding of PLA2 to the interface. Typically, most changes are within 1 log unit; however, the mutants that fall significantly above the line suggest that the NaCl gradient may have an additional effect on the binding along the i-face. Significant changes noted below are interpreted in the context of the structural features of PLA2 (Figure 1).

(a) Relative to WT, the H48 mutants (entries 24−26) have lower isocratic and gradient $t_R$ values. Although the shift for D49E (entry 28) is insignificant, the $t_R$ values are higher

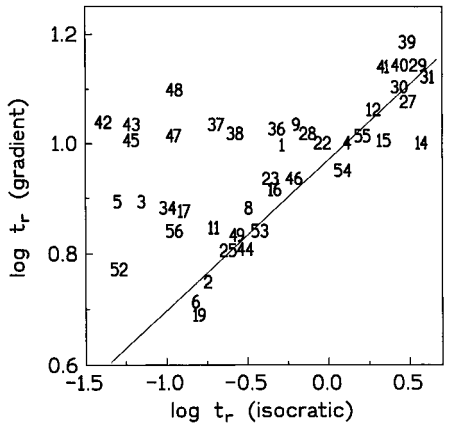


FIGURE 3: Comparison of the retention times for mutants (entries in Table 1) on the IAM-PC column in isocratic 10 mM Tris vs $t_R$ in a reverse linear gradient of NaCl from 2 (up to 2 min) to 0 M (5 min). Note that the void volume has been subtracted from the retention times. In this and subsequent figures, the WT is entry 1, and the line is drawn arbitrarily as a guide for the discussion in the text. Some of the points from Table 1 have been omitted for clarity.

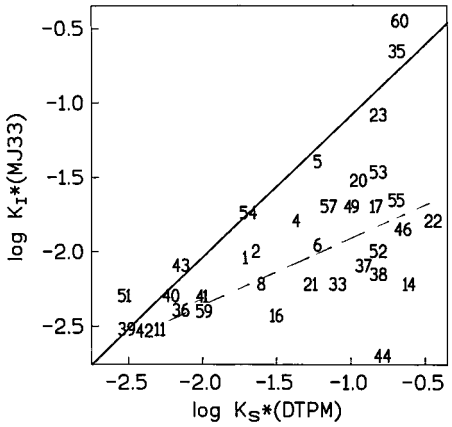


FIGURE 4: Comparison of $K_S$*(DTPM) and $K_I$*(MJ33) for the mutants in Table 1. The WT is entry 1.

for the four nonanionic D49 substitution mutants (entries 27 and 29−31). The carboxylate of D49 provides bidentate oxygen ligand for the seven-coordinate calcium binding, and a weaker binding to D49E is attributed to a four-coordinate calcium (*51*). We suggest that the changes in the retention times for H48 and D49 mutants are due to a perturbed N-terminus; it is connected to H48 via D99 and a structural water molecule, and a mutation of D99 results in a significant shift in Ala1 (*12*). Interfacial binding has an ordering effect on the N-terminal segment (*28*, *52*).

(b) Substitutions on the N-terminus that change both the retention times include L2A (entry 2), L2W (entry 4), W3A (entry 5), Q4 (entries 6−8), and F5 (entries 10−12). In a helical N-terminus, residues A1, Q4, and N6 form a polar face, and L2, W3, and F5 are on a hydrophobic face that lines the substrate binding pocket. A significant increase in the isocratic $t_R$, without a change in the gradient $t_R$, is seen only with N6A (entry 14).

(c) Substitution of K56 by hydrophobic F, I, or M (entries 39−41) increases the gradient and isocratic $t_R$ values. On the other hand, isocratic $t_R$ values are lower, without a significant change in the gradient $t_R$, for K56E (entry 38), K56N (entry 42), and K56T (entry 43). Significantly lower isocratic $t_R$ values are also seen for polar substitutions on Y73 (entries 45, 47, and 48), whereas a hydrophobic substitution, Y73F (entry 46), has little effect. Such changes in the interfacial binding suggest a role for the loop of residues 58−75. Note that as a part of the N-domain, K56 and Y73 could control the contact of the loop with the interface through residues 63−69, and also the N-terminus through the H-bonding network.

(d) Long-range interactions in the N-domain occur through a hydrogen bonding network that includes a highly conserved water. It connects the N-terminal helix to several other residues whose substitution lowers the $t_R$, as in N71E (entry 44), Y52 (entries 33−35), and D99 (entries 50−52).

Collectively, these results imply a coupling between the N-terminus and the loop of residues 58−73 for the binding of PLA2 to the interface. More than 3-fold changes in the extent of interfacial binding are seen with substitutions on F22, the N-terminal helix, K56, Y73, and the loop of residues 58−73. The contribution per substitution for a hydrophobic residue is modest, possibly because, as discussed later, only a fractional surface of the residues along a well-defined i-face makes contact with the interface. The direction of the incremental change induced by individual substitutions is rationalized mostly on the basis of the hydrophobic contacts, although ionic components may also play a role (*31*).

*Calcium Binding.* For most mutants, values of $K_{Ca}$* are within a factor of 3 of that of the WT (results not shown); however, changes in the C-terminus loop have a dramatic effect on the calcium binding to the enzyme in the aqueous phase. The calcium binding loop (residues 26−36), which provides three backbone carbonyl oxygen ligands, is bridged to the C-terminus through a C27−C123 disulfide. The calcium affinity of the E form of C27A/C123A (entry 23) and the C-terminus deletion mutant (entry 60) in the aqueous phase is more than 10-fold lower than that of the WT. On the other hand, their affinity in the E* form is comparable to that for the WT. These and other results (*36*) show that the interface restores the function of a perturbed calcium binding loop, possibly through a contact of L31 with the interface.

*Binding of Substrate Mimics to the Active Site of the E* Form.* The *sn*-2-carbonyl oxygen and the *pro*-*S*-oxygen of the *sn*-3-phosphate group of phospholipid mimic provide two of the seven oxygen ligands for the calcium in the ternary complex E*Ca·L (*10*, *11*, *53*). $K_I$*(MJ33) for the interfacial ternary E*Ca·MJ33 complex (column 6 in Table 1) is a measure of the affinity for a mimic that contains only one acyl chain, and as a tetrahedral mimic without the *sn*-3-phosphate, MJ33 binds to the six-coordinate calcium through its *sn*-2-phosphodiester (*13*). On the other hand, $K_S$*(DTPM) (column 5 of Table 1), DTPM being the ether analogue of the substrate with both the chains, is a measure of the extent of binding to the calcium only through the glycero-*sn*-3-phosphodiester without any contribution from the *sn*-2-carbonyl oxygen.

$K_S$*(DTPM) values for mutants are typically in the mole fraction range of 0.01−0.06, compared to the mole fraction range of 0.006−0.015 for $K_I$*(MJ33). As compared in Figure 4, a modest (<10-fold) discrimination between MJ33 and DTPM persists for the mutants along the dotted line. A significant exception is N71E (entry 44) which, compared to the WT (entry 1), has a significantly lower affinity for DTPM, and a significantly higher affinity for MJ33. It could

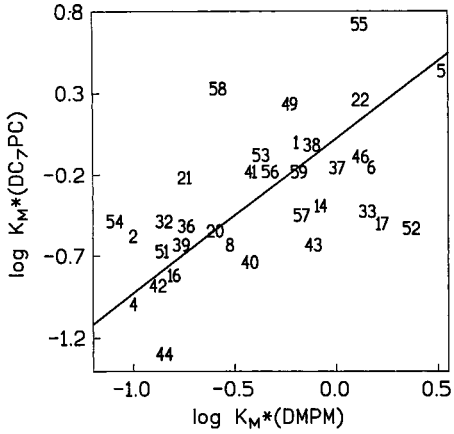


FIGURE 5: Relationship between $K_M$* values for DMPM and DC$_7$-PC for the mutants in Table 1. Larger $K_M$* values are not included. The WT is entry 1.

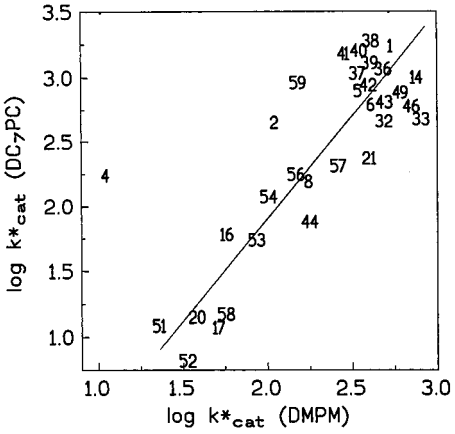


FIGURE 6: Relationship between $k^*_{cat}$(DMPM) and $k^*_{cat}$(DC$_7$PC) in 4 M NaCl for mutants. The WT is entry 1.

be attributable to the binding of *sn*-3-phosphate through Y69 (*19*). Several mutants (entries 5, 23, 35, 39, 43, 51, 54, and 60), above the dotted line and along the solid line in Figure 4, suggest that the affinities for DTPM and MJ33 are comparable. It implies a common feature for the recognition of the two mimics. As a part of the mimic binding pocket, substitutions D99N (entry 51), A102 (entry 53), A103 (entry 55), F5 (entry 11), and W3A (entry 5) change the affinity for both mimics. A large increase in the dissociation constant relative to that of the WT (entry 1) is seen with C27A/C123A (entry 23) and the 115−123 deletion mutant (entry 60), possibly due to a change in the calcium dependence for the mimic binding. The lower affinity of Y52V (entry 35) for both mimics (*26*) may be attributed to a change in the calcium binding through D49 on the preceding turn of the helix. Several K53 (entry 36) and K56 mutants (entries 39−43) have a significantly higher affinity for both the mimics. Overall, these results suggest that multiple factors contribute to the mimic binding, only some of which may be relevant to the substrate binding.

*Interfacial Catalytic Turnover Parameters.* Interfacial $K_M$* values for the hydrolysis of DMPM vesicles (column 8) or DC$_7$PC micelles (column 14) are compared in Figure 5 for some mutants, and others (entries 23, 35, and 60) with $K_M$* values of $\gg$1 are not included. For the mutants along the line with a slope of 1, $K_M$*(DMPM) and $K_M$*(DC$_7$PC) in 4 M NaCl change comparably. Significant departure relative to WT is seen for entries 4, 5, 16, 20, 22, 39, 42, and 51 along the line. On the other hand, a significant departure for one substrate or the other is seen for I9F (entry 17), Y52F (entry 33), D99N/Y52F/Y73F (entry 52), A103S (entry 55), C27A/C123A (entry 23), F106Y (entry 58), and N71E (entry 44). In some cases, mutants with higher $K_S$*(DTPM) values also have higher $K_M$* values. Similarly, lower $K_M$* values for both substrates, points on the lower left side of Figure 5, approach the corresponding $K_S$*(DTPM) values. A change in $K_M$* [$=(k_2^*+k_{-1}^*)/k_1^*$] could be due to a change in $K_S$*-(DTPM) ($=k_{-1}^*/k_1^*$) or $k^*_2$ ($=k^*_{cat}$) because $k_2^* \gg k_{-1}$ (*5*, *45*) and the chemical step is rate-limiting for the WT (*8*). $K_M$* is expected to be larger than $K_S$* as long as $k_2$ is larger than $k_{-1}$. $K_M$* will approach $K_S$* for mutants with low $k^*_{cat}$ values, if $k_1$ and $k_{-1}$ remain unchanged with the substitution. On the basis of similar considerations, higher $K_S$*(DTPM) and $K_M$*(DMPM) values for several substitutions (entries 14, 17, 23, 35, 37, 38, 52, and 55), with little change in $k^*_{cat}$ (see below), are attributed to a decrease in $k_1$* values.

The initial rates of hydrolysis at the maximum substrate mole fraction ($X_S = 1$) of DMPM ($\nu_o$ in column 7 of Table 1) or of DC$_7$PC ($V_M^{app}$ in columns 10 and 13 of Table 1) are related to the intrinsic catalytic turnover parameters (eqs 1 and 3). For most mutants, $V_M^{app}$ in 1 mM NaCl is 10−100-fold lower than in 4 M NaCl. Relative to that of the WT, the rate in 1 mM NaCl is significantly (3−15-fold) higher with hydrophobic K53 and K56 substitutions, and about 2-fold higher for K120A/K121A (entry 59). Higher $V_M^{app}$ values for K53M (entry 37) and K56M (entry 41) at 1 mM NaCl, and virtually the same $V_M^{app}$ at 4 M NaCl as with the WT, have been shown to be due to allosteric $k^*_{cat}$ activation by the interfacial anionic charge (*31*).

The $k^*_{cat}$ values were calculated from $K_M$* and $\nu_o$ or $V_M^{app}$, and plotted in Figure 6. The position for the WT (entry 1) in the upper right corner suggests that virtually all mutants are $k^*_{cat}$-impaired with both substrates. A linear correlation for most mutants suggests that similar structural factors control the chemical step for the two substrates. The most significant exception is L2W (entry 4), which hydrolyzes DMPM at 5% of the rate with DC$_7$PC. Detailed analysis suggests that the indole substituent interferes in the chemical step with the orientation of the longer acyl chain of DMPM (*35*). Although absolute $k^*_{cat}$ values differ by more than a factor of 50, for most mutants $k^*_{cat}$(DC$_7$PC) is about 3.5 times larger than that with DMPM. Despite the fact that one of the substrates is a zwitterionic micelle and the other is an anionic bilayer in the gel phase, we believe that the 3.5-fold difference for the two substrates is dominated by the $k^*_{cat}$ specificity which can be attributed to the headgroup and chain length specificity (*54*), rather than to the effect of the environment due to phospholipid packing.

For mutants with a $K_M$* of <1, a significant change in $\nu_o$ is largely due a change in $k^*_{cat}$ (eq 1). Substitution of catalytic residues D49 and H48 results in virtually a total loss of activity, and D99N substitution results in the loss of >90% of the activity. Other $k^*_{cat}$-impaired mutants include substitutions at D99 (entries 51 and 52), F106 (entries 56−58), A102 (entries 53 and 54), F22A (entry 20), I9F (entry 17), I9A (entry 16), and the N-terminal residues. These residues make contacts with the *sn*-2-acyl chain of the substrate mimics, which is consistent with the substrate specificity in $k^*_{cat}$ observed for the substrate analogues (*42*, *54*).

Collectively, the effect of substitutions on the catalytic parameters suggests that the chemical step of PLA2 is controlled by residues that line the active site slot. Most of the changes in $K_M$* are traced to a change in $k^*_{cat}$ without a significant change in $K_S$* judged as $K_S$*(DTPM). Also, substrate specificity in $k^*_{cat}$ lies in certain specific contacts with the *sn*-2-chain.

*Components of $K_M^{app}$.* According to Scheme 1 and eq 3, $K_M^{app}$ is related to $K_d$, $K_S'$, the cmc of the micellar substrate, and $K_M$ for the monomer path of catalytic turnover (not shown). It is not possible to measure $K_M$ directly, because the rate measured with monodispersed substrate below the cmc is largely an artifact of catalytic turnover at extraneous surfaces of the reaction container and air bubbles (to be published). This relation is valid for bovine PLA2 where $K_S' = 1.5$ mM for $DC_7PC$, $K_S = 3$ mM, $K_M^{app} = 2.3$ mM, and $K_d = 3.2$ mM. This would be expected if $K_M = K_S = 2.5$ mM, as is found to be the case. The validity of eq 3 has been demonstrated for pig pancreatic PLA2 (*2*, *6*), where the binding of substrate mimics to the active site of the E form is driven by the hydrophobic partitioning away from the aqueous phase into the hydrophobic pocket of PLA2 or in a micelle. Thus, with changing NaCl concentrations, the $K_S'/K_S$ ratio for $DC_7PC$ remains constant at about 5, which is consistent with a ratio of 8 calculated from the experimentally measured $K_M$* of 0.07 mole fraction, $K_M^{app}$ of 2.2 mM, and $K_d$ of 3.7 mM at 1 mM NaCl.

## DISCUSSION

Scheme 1 provides a basis for the rationalization of the apparent kinetics with mutants (*23*, *55*) or in complex substrate dispersions (*4*, *9*, *56*). In addition, the microscopic parameters are useful for evaluating specific functional contributions. A set of such primary rate and equilibrium parameters in Table 1, obtained from analysis of the observed kinetics, provides a quantitative basis for the mechanistic and structural interpretation. The set characterizes the microscopic events of interfacial catalysis for the processive turnover at the interface (*3*). The specific effect of a substitution identifies structural features underlying the microscopic event(s). This approach is useful for an energetic representation based on the microscopic functional changes inherent in the primary parameters. We believe that molecular dynamic simulations within the constraints of results in Table 1 will ultimately provide a more detailed picture of catalysis by PLA2. Since such a goal is not within reach yet, we interpret parameters in Table 1 to construct a low-resolution structural basis for the interfacial catalytic turnover, allosteric effects, and processivity. The thermodynamic rationale for this discussion lies in the closed equilibrium relationships, such as the allosteric structural factors that couple the substrate binding to the active site also favoring the binding of the enzyme to the interface (*2*).

*Interfacial Recognition and $K_S$* Allostery*. Identification of the putative i-face is a challenging problem in interfacial enzymology. Structural information about the enzyme at the interface cannot be readily obtained by crystallographic methods; hence, it must be deduced from indirect measurements (*30*, *40*). A unique functional feature of the enzyme at the interface is that it must dislodge the substrate from the interface through an intimate and possibly desolvated

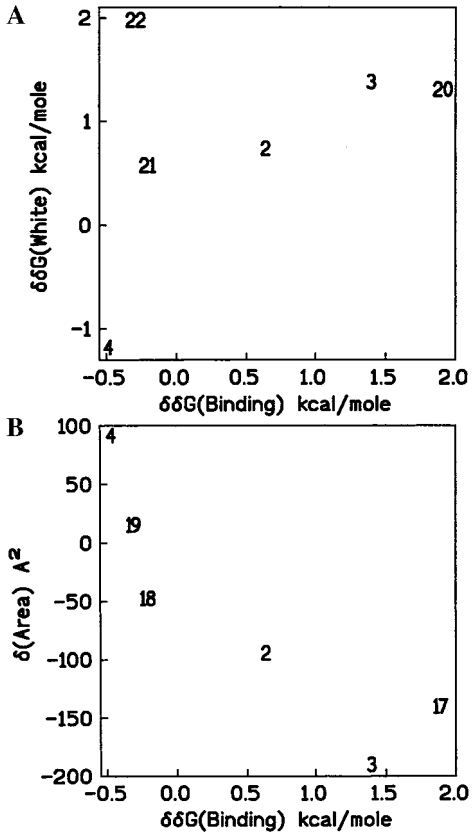


FIGURE 7: Relationship between the incremental free energy for the binding to the IAM surface (ordinate) as a function of (A) the incremental free energies for the binding to the hydrophobic region of the bilayer (*61*) or (B) the change in the hydrophobic area (*58*, *60*) due to the substitution of the residue in the mutant.

contact (*40*). Several residues make up the i-face, and incremental contribution of single substitutions is often modest (*29*, *57*). The degree of plasticity of the interactions at the i-face also remains to be established (*28*, *52*), and such factors, related to the relative sizes of the interacting species (*58*), may skew our linear first-order approximation.

The retention times in Table 1 contain functional information about the i-face. These results clearly establish that PLA2 binds to the interface without the occupancy of the active site. Spectroscopic (*28*, *34*, *40*, *52*, *59*) and kinetic (*23*) evidence suggests a role for the N-terminus in interfacial binding. A less ordered N-terminus seen in the NMR structure of the WT (Figure 1) is consistent with the view that the N-terminus is a part of the i-face. Y52F/Y73F (*43*), D99N (*44*), D99A (*51*), and D99N/Y52F/Y73F (*12*) show a marked perturbation of the N-terminus in their crystal structures, and also a significant decrease in the isocratic retention times. As shown in Figure 7, the incremental free energies for hydrophobic substitutions obtained from $t_R$ values compare reasonably well with the change in the side chain area (*58*, *60*), but not with the incremental energies obtained from the trans-bilayer partitioning or binding of hydrophobic helices (*61*). This behavior is consistent with the suggestion that as a part of the i-face these residues play a role in the hydrophobic interactions involving surface contacts that relate to area. We believe that this strategy may be generally useful for mapping the i-face as well as the substrate binding site.

Binding of PLA2 to the interface is followed by the calcium-dependent binding of the substrate to its active site. Although calcium does not have an effect on the binding of the enzyme to the interface, the affinity of E*Ca·L for the interface is about 100-fold higher (*3*, *6*, *7*). As a part of the thermodynamic cycle intrinsic in Scheme 1, the affinity of E* for a mimic is higher than that of the E form by a factor of 100. It shows a functional coupling between the interfacial binding of the enzyme and the substrate (mimic) binding to the active site. As a structural basis for the $K_S$* allosteric effect of the interface, we believe that the N-terminal segment plays a critical role. Ordering of the N-terminus segment to an amphipathic helix on the binding of the enzyme to the interface could provide the hydrophobic lining for the *sn*-2-chain. $K_S$* and $K_I$* are largely influenced by substitutions that come in direct local contact with the substrate or mimic. A higher intrinsic stability of E*S compared to ES, the $K_S$* allosteric effect of the interface, comes from residues that stabilize the headgroup interactions. In effect, the N-terminal segment could prevent the bound substrate from leaving the active site. Substitutions in the substrate binding site (H48, D49, D99, F22, and F106) also change the binding to the interface. Residues that change $t_R$, $K_S$*, and $K_I$* include L2, F5, N6, I9, F22, Y52, N71, Y73, A102, A103, F106, and possibly the C-terminus. Collectively, a symmetry exists; a local perturbation in the protein structure for the substrate binding is somehow transmitted to the i-face; so does the binding to the interface influence the occupancy of the active site? On the basis of an enhanced calcium-dependent substrate binding to E*, the calcium loop is also an attractive locus for the interface-induced changes in the catalytic parameters.

*Catalytic Turnover*. H48 and D49 are the catalytic residues of PLA2 (*11*, *14*, *15*, *23*). D99 (*11*) and Y69 (*19*) also control $k^*_{cat}$. The catalytic machinery of PLA2 is not functional with the monomeric substrate. PLA2 is modestly active at zwitterionic interfaces, and becomes fully active due to $k^*_{cat}$ activation by the interfacial anionic charge (*6*). Results in Table 1 show that hydrophobic substitution at K53, K56, K120, and K121 increase the rate of hydrolysis at 1 mM NaCl without a significant effect at 4 M NaCl. In terms a two-state model for $k^*_{cat}$ allostery, the inactive form of WT PLA2 at the zwitterionic interface is activated by the charge neutralization either by chloride ion or by an anionic amphiphile in the interface (*31*). On the basis of the results in Table 1, we suggest that charge interactions of PLA2 with the anionic interface, through the cationic residues on the N- and C-domains at the opposite sides of the i-face, make the WT catalytically functional.

*A Heuristic Guide to the Structural Changes on the Binding of PLA2 to the Interface*. There is compelling evidence that the E form undergoes a significant functional change on the binding to interface, and a further change on the mimic binding. The structure in Figure 1 shows that the calcium loop and the N- and C-domains make contact with the interface, and the effect of such changes could be transmitted to the catalytic site through the N-terminus. The crystallographic structure of the ECa and the ECaI complex of PLA2 are virtually identical (*11*, *13*), yet noticeably different from the NMR structure for the E form (*20*−*22*). Note that the NMR structure on alkylphosphocholine micelles (*21*, *22*) represents a mixture of E* and E*I species because the amphiphiles binds to the active site (*41*). With its more disordered features, the NMR structure of the E form provides a reference basis for evaluating the possible changes associated with the events of interfacial catalysis. Thus, structural features of interest for the interfacial effects on the catalytic turnover include the following.

(a) The pucker in the calcium loop of residues 25−36 could account for differing calcium and inhibitor affinities for the E versus E*Ca forms. A role for the C-terminus in calcium and substrate binding (*36*) is also consistent with differences in the precise geometry of these residues coupled to the calcium loop via the disulfide bridge of residues 27−123 in the C-domain.

(b) As a possible contribution to $K_S$* allostery, note that the helix of residues 17−22 involved in the mimic binding in ECaI structure is absent in the NMR structure. Also, L2, W3, L31, F22, and F106 become more ordered and thus better able to accommodate the hydrophobic region of the substrate in the active site.

(c) Control of $k^*_{cat}$ by the interfacial anionic charge through charge neutralization of K53 and K56 could make the loop of residues 58−75 more ordered to make contact with the interface. This is consistent with the fact that Y69, N71, and Y73 substitutions impair $k^*_{cat}$. A mechanism of allosteric control by a loop at the contact site between two subunits is suggested for fructose 1,6-bisphosphatase (*62*).

(d) Binding to the interface involves several residues, and thus, the effect of individual substitutions is expected to be modest. The largest change in $K_d$ (Figure 3) with the K56 substitution can be attributed to the ordering of the loop of residues 58−75. For example, it could enhance the hydrophobic contact of the interface with the sequence of residues 63−65 (FLV).

To recapitulate, functional parameters are useful in identifying not only a role for specific residues but also the topological distribution of residues which is useful for identifying contributions of segments, and C- and N-domains in events of the interfacial catalytic cycle of PLA2. Our interpretation of the short- and long-range effects is based on the heuristic that the effect of a structural perturbation on a function implies that a functional change must accompany a complementary structural change. Modest incremental changes associated with the substitutions at key positions effectively dissect the functional changes in terms of the primary rate and equilibrium parameters. Our results show a functional coupling between the catalytic and interfacial binding events is associated with specific residues. Finally, the strategy for looking at multiple mutations with a modest effect of each is particularly apt for evaluating functional contributions while minimizing the effect of major structural perturbations.

## REFERENCES

1. Jain, M. K., Rogers, J., Jahagirdar, D. V., Marecek, J. F., and Ramirez, F. (1986) *Biochim. Biophys. Acta 860*, 435−447.
2. Jain, M. K., Yu, B.-Z., and Berg, O. G. (1993) *Biochemistry 32*, 11319−11329.
3. Jain, M. K., Gelb, M. H., Rogers, J., and Berg, O. G. (1995) *Methods Enzymol. 249*, 567−614.
4. Jain, M. K., and Berg, O. G. (1989) *Biochim. Biophys. Acta 1002*, 127−156.
5. Berg, O. G., Yu, B.-Z., Rogers, J., and Jain, M. K. (1991) *Biochemistry 30*, 7283−7297.

6. Berg, O. G., Rogers, J., Yu, B., Yao, J., Romsted, L. S., and Jain, M. K. (1997) *Biochemistry 36*, 14512−14530.
7. Berg, O. G., Cajal, Y., Butterfoss, R. L., Grey, R. L., Alsina, M. A., Yu, B. Z., and Jain, M. K. (1998) *Biochemistry 37*, 6615−6627.
8. Jain, M. K., Rogers, J., Gelb, M. G., Tsai, M.-D., Hendrickson, E. K., and Hendrickson, S. (1992) *Biochemistry 31*, 7841−7847.
9. Jain, M. K., Rogers, J., Hendrickson, H. S., and Berg, O. G. (1993) *Biochemistry 32*, 8360−8367.
10. Thunnissen, M. M. G. M., Ab, E., Kalk, K. H., Drenth, J., Dijkstra, B. W., Kuipers, O. P., Dijkman, R., de Haas, G. H., and Verheij, H. M. (1990) *Nature 347*, 689−691.
11. Scott, D., and Sigler, P. (1994) *Adv. Protein Chem. 45*, 53−88.
12. Sekar, K., Yu, B. Z., Rogers, J., Lutton, J., Liu, X., Chen, X., Tsai, M. D., Jain, M. K., and Sundaralingam, M. (1997) *Biochemistry 36*, 3104−3114.
13. Sekar, K., Eswaramoorthy, S., Jain, M. K., and Sundaralingam, M. (1997) *Biochemistry 36*, 14186−14191.
14. Verheij, H. M., Volwerk, J. J., Jansen, E. H. J. M., Puijk, W. C., Dijkstra, B. W., Drenth, J., and de Haas, G. H. (1980) *Biochemistry 19*, 743−740.
15. Verheij, H. M., Slotboom, A. J., and de Haas, G. H. (1981) *Rev. Physiol. Biochem. Pharmacol. 91*, 91−203.
16. Volwerk, J. J., Pieterson, W. A., and de Haas, G. H. (1974) *Biochemistry 13*, 1446−1454.
17. Yu, B. Z., Berg, O. G., and Jain, M. K. (1993) *Biochemistry 32*, 6485−6492.
18. Yu, B. Z., Rogers, J., Ranadive, G., Baker, S., Wilton, D. C., Apitz-Castro, R., and Jain, M. K. (1997) *Biochemistry 36*, 12400−12411.
19. Yu, B. Z., Rogers, J., Nicol, G. R., Theopold, K., Seshadri, K., Vishweshwara, S., and Jain, M. K. (1998) *Biochemistry 37*, 12576−12587.
20. Yuan, C., Li, Y., Byeon, I., Poi, M., and Tsai, M. D. (1999) *Biochemistry 38*, 2919−2929.
21. Van den Berg, B., Tessari, M., de Haas, G. H., Verheij, H. M., Boelens, R., and Kaptein, R. (1995) *EMBO J. 14*, 4123−4131.
22. Van den Berg, B., Tessari, M., Boelens, R., Dijkman, R., Kaptein, R., de Haas, G. H., and Verheij, H. M. (1995) *J. Biomol. NMR 5*, 110−121.
23. Verheij, H. M. (1995) in *Phospholipase $A_2$ in Clinical Inflammation* (Glaser, K. B., and Vadas, P., Eds.) pp 3−24, CRC Press, Boca Raton, FL.
24. Gelb, M. H., Jain, M. K., Hanel, A. M., and Berg, O. G. (1995) *Annu. Rev. Biochem. 64*, 653−688.
25. Li, Y., Yu, B. Z., Zhu, H., Jain, M. K., and Tsai, M. D. (1994) *Biochemistry 33*, 14714−14722.
26. Dupureur, C. M., Yu, B.-Z., Jain, M. K., Noel, J. P., Deng, T., Li, Y., Byeon, I. L., and Tsai, M. D. (1992) *Biochemistry 31*, 6402−6413.
27. Dupureur, C. M., Yu, B.-Z., Mamone, J. A., Jain, M. K., and Tsai, M. D. (1992) *Biochemistry 31*, 10576−10583.
28. Jain, M. K., and Maliwal, B. P. (1993) *Biochemistry 32*, 11838−11846.
29. Ghomashchi, F., Lin, Y., Hixon, M. S., Yu, B. Z., Annand, R., Jain, M. K., and Gelb, M. G. (1998) *Biochemistry 37*, 6697−6710.
30. Lin, Y., Nielsen, R., Murray, D., Hubbell, W. L., Mailer, C., Robinson, B. H., and Gelb, M. H. (1998) *Science 279*, 1925−1929.
31. Rogers, J., Yu, B. Z., Tsai, M. D., Berg, O. G., and Jain, M. K. (1998) *Biochemistry 37*, 9549−9556.
32. Noel, J. P., Bingman, C. A., Deng, T., Dupureur, C. M., Hamilton, K. J., Jiang, R., Kwak, J., Sekharudu, C., Sundaralingam, M., and Tsai, M. D. (1991) *Biochemistry 30*, 11801−11811.
33. Li, Y., and Tsai, M. D. (1993) *J. Am. Chem. Soc. 115*, 8523−8526.
34. Zhu, H., Dupureur, C. M., Zhang, X., and Tsai, M. D. (1995) *Biochemistry 34*, 15307−15314.
35. Liu, X., Zhu, H., Huang, B., Rogers, J., Yu, B. Z., Kumar, A., Jain, M. K., Sundaralingam, M., and Tsai, M. D. (1995) *Biochemistry 34*, 7322−7334.
36. Huang, B., Yu, B. Z., Rogers, J., Byeon, I. L., Sekar, K., Chen, X., Sundaralingam, M., Tsai, M. D., and Jain, M. K. (1996) *Biochemistry 35*, 12164−12174.
37. Apitz-Castro, R. J., Jain, M. K., and De Haas, G. H. (1982) *Biochim. Biophys. Acta 688*, 349−356.
38. De Araujo, P. S., Rosseneu, M. Y., Kremer, J. M. H., van Zoelen, E. J. J., and de Haas, G. H. (1979) *Biochemistry 18*, 580−586.
39. Dijkstra, B. W., Drenth, J., and Kalk, K. H. (1981) *Nature 289*, 604−606.
40. Ramirez, F., and Jain, M. K. (1991) *Proteins: Struct., Funct., Genet. 9*, 229−239.
41. Jain, M. K., Tao, W., Rogers, J., Arenson, C., Eibl, H., and Yu, B.-Z. (1991) *Biochemistry 30*, 10256−10268.
42. Jain, M. K., and Rogers, J. (1989) *Biochim. Biophys. Acta 1003*, 91−97.
43. Sekharudu, C., Ramakrishnan, B., Huang, B., Jiang, R. T., Dupureur, C. M., Tsai, M. D., and Sundaralingam, M. (1992) *Protein Sci. 1*, 1585−1594.
44. Kumar, A., Sekharudu, C., Sekharudu, Y. C., Dupureur, C. M., Zhu, H., Tsai, M. D., and Sundaralingam, M. (1994) *Protein Sci. 3*, 2082−2088.
45. Jain, M. K., Yu, B.-Z., Rogers, J., Ranadive, G. N., and Berg, O. G. (1991) *Biochemistry 30*, 7306−7317.
46. Bayburt, T., Yu, B. Z., Street, I., Ghomashchi, F., Laliberte, F., Perrier, H., Wang, Z., Homan, R., Jain, M. K., and Gelb, M. K. (1995) *Anal. Biochem. 232*, 7−23.
47. Ong, S., Liu, H., and Pidgeon, C. (1996) *Biochim. Biophys. Acta 905*, 1−8.
48. Pidgeon, C., and Venkatarum, U. V. (1989) *Anal. Biochem. 67*, 3550−3557.
49. Fairbanks, R. W. P., and Wirth, M. J. (1997) *Anal. Chem. 69*, 2258−2261.
50. Jain, M. K., Egmond, M. R., Verheij, H. M., Apitz-Castro, R. J., Dijkman, R., and de Haas, G. H. (1982) *Biochim. Biophys. Acta 688*, 341−348.
51. Sekar, K., Biswas, R., Li, Y., Tsai, M. D., and Sundaralingam, M. (1999) *Acta Crystallogr. D55*, 443−447.
52. Maliwal, B. P., Yu, B. Z., Szacinski, H., Squier, T., Van Binsbergen, J., Slotboom, A. J., and Jain, M. K. (1994) *Biochemistry 33*, 4509−4516.
53. Tsai, T. C., Hart, J., Jiang, R., Bruzik, K., and Tsai, M. D. (1985) *Biochemistry 24*, 3180−3188.
54. Rogers, J., Yu, B. Z., Serves, S. V., Tsivgoulis, G. M., Sotiropolos, D. N., Ioannou, P. V., and Jain, M. K. (1996) *Biochemistry 35*, 9375−9384.
55. Dua, R., Wu, S. K., and Cho, W. (1995) *J. Biol. Chem. 270*, 263−268.
56. Homan, R., and Jain, M. K. (1999) in *Intestinal Lipid Metabolism* (Mansbach, C. M., Ed.) Plenum, New York (in press).
57. Snitko, Y., Koduri, R. S., Han, S. K., Molini, B. J., Wilton, D. C., Gelb, M. H., and Cho, W. (1997) *Biochemistry 36*, 14325−14333.
58. Sharp, K. A., Nicholis, A., Friedman, R., and Honig, B. (1991) *Biochemistry 30*, 9686−9697.
59. Jain, M. K., Maliwal, B. P., de Haas, G. H., and Slotboom, A. J. (1986) *Biochim. Biophys. Acta 860*, 448−461.
60. Beal, R. E., Toscana-Cantaffa, D., Young, P., Rechsteiner, M., and Pickert, C. M. (1998) *Biochemistry 37*, 2925−2934.
61. Wimpley, W. C., and White, S. H. (1996) *Nat. Struct. Biol. 3*, 842−848.
62. Choe, J., Poland, B. W., Fromm, H. J., and Honzatko, R. B. (1998) *Biochemistry 37*, 11450−11450.


BI982215F